Conductance oscillations related to the eigenenergy spectrum of a quantum dot in weak magnetic fields

M. Persson and J. Pettersson
Department of Physics, Chalmers University of Technology and University of Göteborg, S-412 96 Göteborg, Sweden

B. von Sydow
Department of Applied Physics, Chalmers University of Technology and University of Göteborg, S-412 96 Göteborg, Sweden

P. E. Lindelof and A. Kristensen
Niels Bohr Institute, University of Copenhagen, Universitetsparken 5, Dk-2100 Copenhagen, Denmark

K. F. Berggren
Department of Physics and Measurement Technology, Linköping University, S-581 83 Linköping, Sweden
(Received 17 November 1994)

The electron transport through a quantum dot, defined by the electrostatic potential of four Schottky gates on top of a GaAs-$Ga_xAl_{1-x}As$ heterostructure, was studied experimentally. The dot was connected to the surrounding two-dimensional electron gas by two variable quantum point contacts. The conductance, measured either as a function of gate voltage or magnetic field, showed characteristic variations: conductance maxima recurrently appear when the gate voltage is varied and conductance maxima are observed to shift approximately linearly in position when the magnetic field is varied. The measurement is compared with a transport model, where the eigenenergy spectrum is calculated for an isolated perfectly circular disk, with qualitative agreement regarding the characteristic variations of conductance and in Fourier power spectra of magnetoconductance. The conductance variations are related to the density of states at the Fermi energy. They cannot be attributed to single levels because the number of electrons in the dot was too large (approximately 1700 electrons), but originate from a shell structure with coincident energy levels.

I. INTRODUCTION

The low electron density and extreme purity of materials grown by molecular-beam epitaxy make it possible to study quantum coherence effects in structures smaller than elastic scattering lengths and characteristic phase coherence lengths. A very small conducting island, a quantum dot, can be defined in a two-dimensional electron gas (2DEG) by limiting its extensions with an electrostatic field. It is often compared with an artificial atom, having a fixed number of electrons and a discrete eigenenergy spectrum.[1,2] The spectra of quantum dots have been investigated by transport measurements with high resistance of the point contacts in the tunneling regime, with only a few Landau levels in the dot[3–5] and by capacitance measurements of a dot containing only a few electrons.[2,6] In both cases a general agreement between the measured spectra and the spectrum of a two-dimensional harmonic oscillator is found. The spectrum is very complex with frequent crossings of single-particle levels, when the number of electrons in the dots is large and when the magnetic field is weak. The quantum dots studied in this work were large, with approximately 1700 electrons. We will in this paper compare measured conductance variations with a quantum-mechanical model of perfect model geometry, namely, a circular disk, and analyze the regularities of these conductance variations at low magnetic fields.

The electron transport behavior of ballistic microstructures has been analyzed using "billiard ball" models,[7] where the electrons move as classical particles and bounce against the confining walls but carry phase information allowing for quantum interference. When the electron moves in a closed trajectory in a magnetic field, the phase change along the loop is determined by the enclosed flux, and the conductance is periodic in the magnetic flux quantum h/e. This causes the conductance of a quantum dot to vary nonmonotonically when the magnetic field or the gate voltages change. The variations resemble universal conductance fluctuations that appear in disordered conductors. In ballistic quantum dots, however, the variations are due to the geometry of the confinement potential and not to randomly distributed scatterers.

The occurrence of chaos in quantum systems has recently been frequently discussed.[8–16] Classical electron scattering is chaotic for the case of asymmetric or distorted geometries, in the sense that an electron orbit is extremely sensitive to initial conditions. The variations of conductance will in that case be aperiodic. The statistical properties of chaotic fluctuations have been predicted from scattering dynamics.[8] The difference between a chaotic and a nonchaotic (circular) geometry was investigated experimentally by Marcus *et al.*[12] They found a difference in the Fourier power spectrum of magnetoconductance for the different geometries. The amplitude of

0163-1829/95/52(12)/8921(13)/$06.00

low-frequency components was the same, but for higher frequencies the difference appears as higher amplitudes for the circular geometry compared to the stadium-shaped (chaotic) structure.

Stone and Bruus[10] have found that minor distortions of the boundary may dramatically change calculated energy levels of a quantum dot. The question is then raised of whether a comparison between calculated energies and eigenstates for a perfectly shaped geometry is relevant to explain an experimental reality. The boundary of the electrostatic confinement is always slightly distorted, the regions around the contacts are definitely not a regular geometry, and elastic scattering events change the direction of electron paths.

Single-electron effects are important in semiconductor quantum dots. The incremental charging of a dot that is weakly coupled to its environment (the tunneling regime) results in periodic conductance peaks, referred to as Coulomb blockade oscillations. Irregular variations of the amplitude of Coulomb blockade oscillations at weak magnetic field have been reported by Staring *et al.*[17] They are explained in terms of chaotic fluctuations of tunnel rates by Jalabert, Stone, and Alhassid.[9] This work consists of an experimental study of the conductance of circularly-shaped quantum dots, confined in a 2DEG by the electrostatic potential of four individually adjustable gates. The two-terminal conductance was measured as a function of gate voltage, magnetic field, and temperature. We observe characteristic variations that can be explained by a transport model, where the electrons tunnel from one reservoir, through the discrete states of an isolated perfectly circular disk, to another reservoir. The peak values of the Fourier power spectra of magnetoconductance are high for low-frequency components and decrease stepwise for frequencies higher than $1/\Delta B = \pi a^2 e/h$, corresponding to additions of magnetic flux quanta to the dot of radius a.

We show that a perfectly shaped model geometry is in reasonable agreement with experimental results, that is, the observed regular variations can be described with a nonchaotic model. The observed variations are related to variations in the density of states at the Fermi energy, which, in turn, is related to the zeros of Bessel functions.

II. SAMPLE PREPARATION AND EXPERIMENTAL DETAILS

The samples were fabricated using GaAs-$Ga_xAl_{1-x}As$ heterostructures grown by molecular-beam epitaxy. A high mobility 2DEG forms at the GaAs-$Ga_xAl_{1-x}As$ interface. The sheet electron density was $n_s = 3.7 \times 10^{15}$ m^{-2} and the mobility of the sample μ was 63 m^2/V s at 9 K, determined from measurements of the low-field Hall effect and the longitudinal resistance. The elastic mean free path $l = \mu h/e\lambda_F = 6$ μm, where λ_F is the Fermi wavelength. The heterostructure with the gate structure on top is schematically shown in Fig. 1.

A mesa was etched on the 2DEG to isolate an active region. The mesa, the AuGeNi Ohmic contacts, the aligning marks, and the contact pads were patterned with photolithographic processes. The Schottky gates (150 Å Ti/150 Å Au) were made with electron-beam lithography and lift-off.

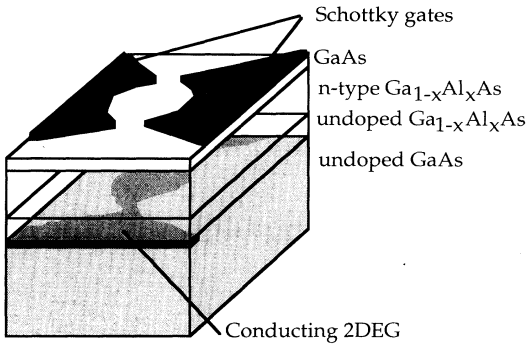

FIG. 1. Schematic layer configuration of the heterostructure. A high mobility 2DEG forms in the undoped GaAs at the interface to the $Ga_xAl_{1-x}As$ layer. The 2DEG is separated from the randomly distributed donors in the $Ga_xAl_{1-x}As$ by an undoped spacer layer. A negative voltage V_g on the gates depletes the 2DEG beneath the gates.

We used a double-layer electron-beam resist. The bottom layer was copolymer *p*[MAA-MMA] (poly[methacrylic acid-methylmethacrylate]) and the top layer was PMMA (polymethylmethacrylate). They were spun on the substrate and baked on a hot plate in two steps. The bottom layer thickness was $\approx$120 nm and the top layer was $\approx$70 nm. The double layer was, after exposure, developed in a PMMA developer (toluene: isopropanol, 1:3) and a copolymer developer (2-ethoxiethylacetate: ethanol, 1:5) successively. A linewidth of 40 nm has been achieved with this resist configuration.

The geometry of the gate structure is seen in the scanning electron microscope (SEM) imagine in Fig. 2. Only two gate pairs were used at a time in the experiments, while the third pair was unconnected or grounded and did not affect the measurement. The gate voltages on the electrodes were varied in pairs. The voltage on the middle gate pair V_{g2} was swept, while the voltage on the other pair was constant. The gate voltage affects not only the width of the channel, and thereby the conductance of the quantum point contact, but also the area of the dot that is confined between the gate pairs. Taking into account that the depletion region in the 2DEG is slightly larger than the extent of the gate, the diameter of the quantum dot is approximately 0.8 μm.

The current and the voltage over the sample were measured with ac lock-in amplifiers and the two-terminal conductance was calculated from these values. Differential preamplifiers were mounted on top of the cryostat. The sample was biased symmetrically by an ac voltage over two 100-kΩ resistors in series with the sample. The voltage over the sample was less than 10 μV, but changed as the sample resistance changed. The gate voltages were applied relative to 0-V bias voltage, thus the bias sweep had a minimal influence on the depletion of the 2DEG. The sample was bonded and mounted on a Si carrier chip, which was contacted by metallic spring-loaded pins in the sample holder. The sample was loaded

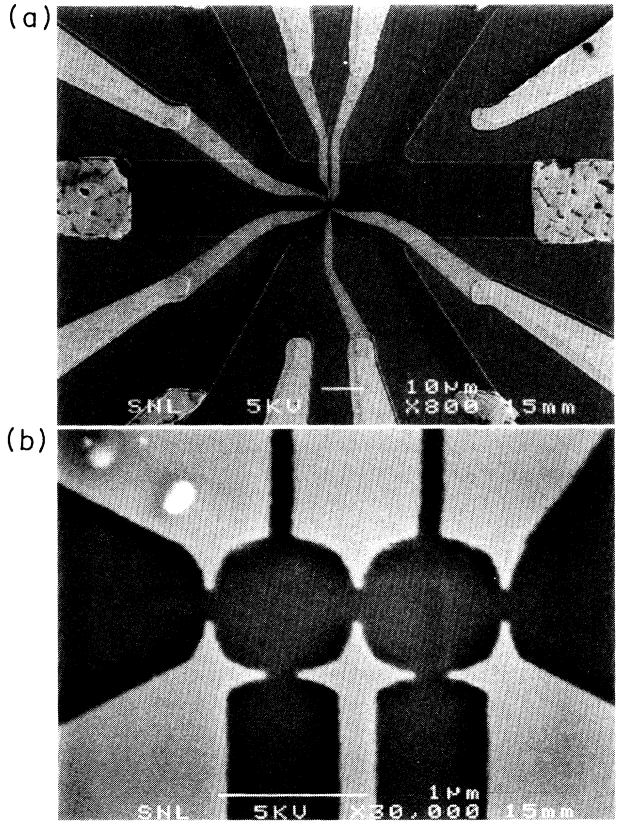

FIG. 2. (a) Scanning electron microscope (SEM) image of the device with gates and Ohmic contacts shown. (b) SEM image of the gate structure. Two gate pairs were used during the measurements, the third was grounded or disconnected. The gate voltages V_{g1}, V_{g2}, and V_{g3} referred to in the text are the voltages applied to the two right gates, to the middle gates, and to the left gates, respectively. The gates can form three individually adjustable quantum point contacts and two circularly shaped quantum dots.

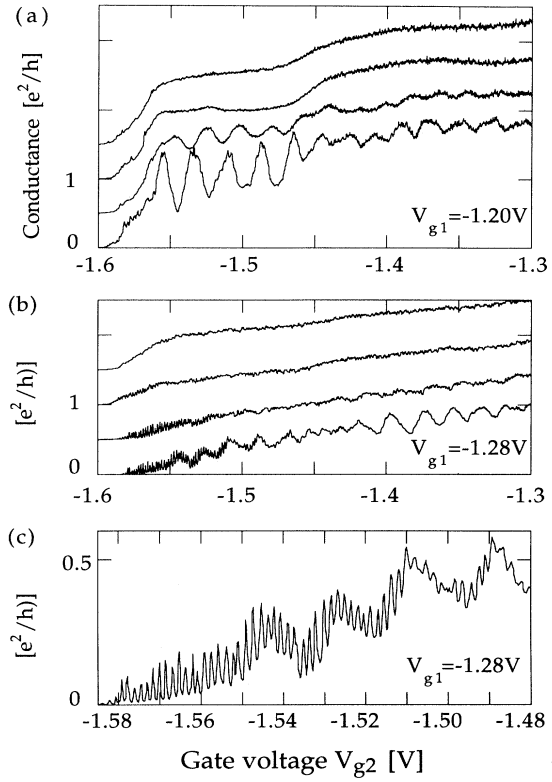

FIG. 3. Conductance oscillations at $B=1$ T. The long period oscillations are due to additions of single flux quanta to the dot. Single electron charging results in the short period (Coulomb blockade) oscillations, that are superposed on the long period oscillations in the low conductance limit. The conductance is measured at four different temperatures, from top $T=2.0$, 0.8, 0.3, and 0.045 K, for (a) $V_{g1}=-1.20$ V and (b) $V_{g1}=-1.28$ V. (c) An expansion of the 45-mK trace from (b), where Coulomb blockade oscillations are resolved.

into a dilution refrigerator that had a base temperature of ≈ 15 mK. Magnetic fields up to $B=5$ T could be applied perpendicular to the substrate. The conductance was measured as a function of V_{g2} (changing the dot size), or as a function of magnetic field, at different settings of the other gate pairs and at different temperatures.

III. EXPERIMENTAL RESULTS

The conductance of a one-dimensional channel (or point contact) depends upon the number of conducting subbands, each with a conductivity of $2e^2/h$, that are allowed.[18] The development of the conductance of the dot and its contacts as one of the point contacts is opened up is most clearly seen in the two upper traces of Fig. 3(a). (The other point contact is already open and its size is kept unchanged.) The channel is pinched off and there is no conductance when a large negative voltage is applied to gate pair 2 ($V_{g2}<-1.6$ V). The first channel opens up and the conductance increases towards $2e^2/h$ as the magnitude of V_{g2} decreases. At a somewhat larger V_{g2}, a second channel opens up and the conductance increases another step in the conductance staircase. (Note that the observed conductance is the one of the two point contacts in series. This may explain the magnitude of the steps.)

Charging effects are important when the conductances of both point contacts are less than the conductance quantum value $2e^2/h$. We will disregard charging effects after treating them briefly in Sec. III A. Instead, we will concentrate on the magnetoconductance behavior as the size of the dot is varied, when at least one point contact is above $2e^2/h$ in conductance.

At large magnetic fields, when the classical cyclotron radius ($r_c=\Phi_0/\lambda_F B$), where $\Phi_0=h/e$, λ_F is the Fermi wavelength, and B is the magnetic flux density) is smaller than the dot radius, skipping orbits or edge states will dominate the conductance behavior. At sufficiently large field, there is no scattering between edge states as argued by Glazman and Jonson,[19] and the dot behaves essentially as a ring giving rise to Aharonov-Bohm[20] oscillations with well-defined period in magnetic flux. The high-magnetic-field case is the one that has been most thoroughly studied. In the opposite regime, at small fields, the electrons are described as waves bouncing

against the walls of the dot. The bounces will depend critically upon initial conditions (like the widths of the entrance and the exit channels) and inhomogeneities in the wall geometry. One does not expect periodic variations in the conductance with magnetic field or with dot size, as for the large field case, but rather aperiodic fluctuations like the conductance variations in a mesoscopic conductor.[21] We will concentrate on the behavior in this low-field regime and show that the conductance is not completely chaotic but that there exist pronounced regularities in its response to changes in field and dot size.

A. Coulomb blockade oscillations

Charging effects are important when the conductances of both point contacts are less than the conductance quantum $2e^2/h$. The periodically appearing conductance peaks in Fig. 3(c) are Coulomb blockade oscillations, due to the incremental charging of the island by single electrons. This phenomenon has been observed by several groups[22] and single-electron effects in semiconductors are reviewed by van Houten, Beenakker, and Staring.[23] The coupling capacitance between the gate and the dot can be determined from the average period between the peaks $\Delta V_g = e/C_g$. For V_{g2} the average period was 1.7 mV and the corresponding capacitance to one gate pair was $C_{g2} \approx 9 \times 10^{-17}$ F. The positions of the peaks are not truly periodic, but slightly shifted due to the spacing between successive energy levels. The difference between single-electron energies can be extracted from the peak positions, by subtracting the average period corresponding to the charging energy. The method has been used to map the energy spectrum in the quantum Hall regime.[3,5]

The single-electron charging of the island creates a renormalized energy spectrum where the single-electron levels are separated by the bare level spacing and the charging energy, $\Delta E^* = \Delta E + e^2/C$.[23] The following measurements are performed when the conductance of one point contact varies from 0 to $\sim 4e^2/h$. The charging of the island only affects the measurement when the conductance of both point contacts is less than $2e^2/h$, that is, in the region where Coulomb blockade oscillations are observed.

B. Measurements in high magnetic field

The conductance of a quantum dot oscillates periodically as a function of magnetic field or size of the dot, when Landau-level edge states are formed in high magnetic fields.[24] The period is determined by the magnetic flux enclosed by the edge states.

The long period oscillations seen in Fig. 3(a) are due to a variation of the area. Each period corresponds to a change of flux within the edge state by one flux quantum $\Phi_0 = h/e$. The area change is $\Delta A = h/eB$ for each period (at 1 T, $\Delta A = 4.1 \times 10^{-15}$ m^2). We can therefore determine the variation of the area induced by the gate voltage. The radius changes $\Delta r = 1.6$ nm for each flux quantum at $B = 1$ T, if the dot radius is 0.4 μm. The relation between Δr and the gate voltage is then $\Delta r/\Delta V_{g2} = 0.07$ μm/V obtained from the data of Fig. 3. All presented measurements are performed with the same sample, but it has been thermally cycled and stored in air between measurements. We assume that the relation between size and gate voltage has changed insignificantly between the measurements.

The long period oscillation and the Coulomb blockade oscillation are superposed when the conductances of both point contacts are low; see Figs. 3(b) and 3(c). Staring *et al.*[17] measured and explained a periodic envelope of Coulomb blockade oscillations in a quantum dot and found the number of Coulomb blockade peaks in each period of the envelope to be inversely proportional to the magnetic field. The Landau levels are filled sequentially; one electron enters each of the Landau levels when one magnetic flux quantum is added to the dot. The transport process involves tunneling to the outermost level followed by an equilibration to the inner Landau levels. The amplitude variation is explained as due to variations of the tunneling probability to predominantly the outermost Landau level. A similar behavior has been observed in this dot, with the long period oscillation as a function of gate voltage inversely proportional to the magnetic field.[25]

The amplitude of Coulomb blockade oscillations diminishes at high point contact conductance, and only the long period oscillation remains. Long period conductance variations also appear at lower fields and even at zero field. These variations are not as periodic as those at higher field.

Both kinds of oscillations have a similar temperature dependence (Fig. 3). The increase of the amplitudes ceases below 0.2 K. This may be related to a difference between the mixing chamber temperature and the effective electron temperature. We believe that the electron temperature is not lower than about 100–200 mK, even when the mixing chamber is at base temperature 15 mK. Meirav *et al.*[14] have also found that the electronic temperature fails to reach temperatures below 100 mK. They match the shape of Coulomb blockade peaks to the derivative of the Fermi-Dirac distribution function to obtain a more precise estimate of the effective temperature.

The number of modes in one quantum point contact changes when the gate voltage is varied. This can be seen in Fig. 3(a) at $T = 2$ K where the conductance has two steps, indicating that the number of modes changes from zero to two in that gate voltage interval.

C. Measurements in weak magnetic field

Conductance variations were also seen at low magnetic field, even at zero field. Nonmonotonic variations of the conductance are seen in Fig. 4, as a function of gate voltage on one gate pair, at $B = 0$ mT. They have an amplitude that is considerably larger than the one of the Coulomb blockade oscillation. We will argue that they are due to variations in the density of states at the Fermi energy. The energy spectrum of the dot is not affected by the charging energy at gate voltages higher than $V_{g2} = -1.45$, where the conductance of the swept point contact is estimated to be higher than $2e^2/h$. The spectra obtained by McEuen *et al.*[5] and Ashoori *et al.*[6] are

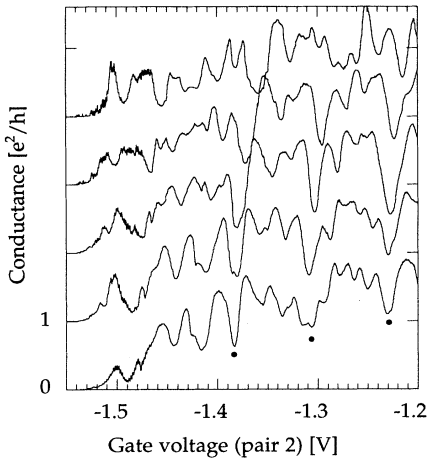

FIG. 4. Conductance oscillations as a function of V_{g2} at $B=0$ T, $T=15$ mK. The other gate pair is in the lowest trace at $V_{g3}=-1.180$ V and is changed with -12 mV for each of the offset traces to -1.228 V in the top trace. Both the area of the dot and the width of the point contact increase, when the V_{g2} is swept.

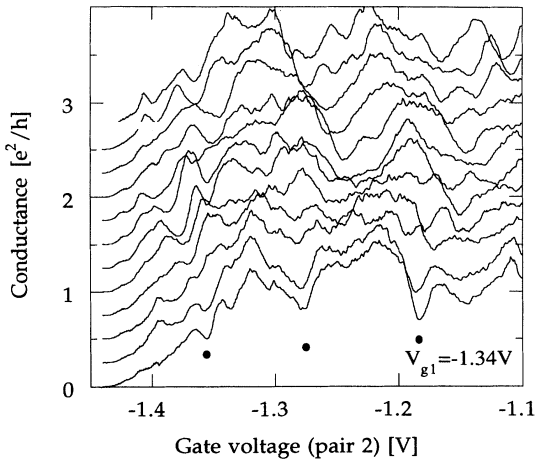

FIG. 5. Conductance oscillations as functions of V_{g2} for fixed $V_{g1}=-1.34$ V. The magnetic field is $B=0$ mT in the bottom trace and increases in steps of 4 mT for each trace to 44 mT. Prominent equidistant dips appear marked with dots in the zero-magnetic-field trace. The Coulomb blockade regime, where charging effects have to be accounted for, is estimated to be below $V_{g2}\approx -1.35$ V. $T\approx 20$ mK.

both measured in the Coulomb blockade regime, where the charging energy has to be taken into account. The geometric form of the dot changes somewhat between the different traces, but despite this some structure remains. Three large dips (marked with dots), with about the same separation in gate voltage, can be seen in all traces. A fourth smaller dip can be seen in the Coulomb blockade regime, but the separation to that dip is larger. This periodicity is one of the characteristics that can be explained with our simple transport model that will be described in Sec. IV.

The two-terminal conductance is shown in Fig. 5 for the second dot of the same sample (see Fig. 2), but measured nine months later. Any configuration of scatterers is therefore not the same. Three dips appear at equidistant position also in this measurement. These are marked by dots in the figure. The oscillation changes drastically when a weak magnetic field is applied. No correlation between the different sweeps is obvious, even though the magnetic field step is only 4 mT between the different traces. The correlation, however, can be seen when the data of Fig. 5 are displayed as a grey-scale image of the conductance as a function of the swept gate voltage and the magnetic field in 1-mT steps; see Fig. 6(d). A third-order polynomial is subtracted from each sweep to make the oscillatory behavior more visible and remove the effect of the increasing conductance of the point contact. Four grey-scale pictures are shown. They are taken with a change of 10 mV of V_{g1}, between the different images. Bright and dark regions denote maxima and minima in the conductance, respectively. We observe a characteristic pattern in the four images. Three or four dark regions appear at zero magnetic field in Figs. 6(a)–6(d) corresponding to the dips with low conductance in Fig. 5. Moreover, three bright regions with high conductance can be observed. The patterns shift and change slightly for the different settings of V_{g1}, but the general features can still be recognized in the different images; i.e., the behavior is not chaotic. There are diagonal features that appear approximately periodic, like a wave pattern. Diagonal dark and bright regions can be seen in the upper part of the images. They are separated by a smaller distance than the dips mentioned above.

Characteristic features, e.g., dark spots at zero magnetic field, can be seen in all four grey-scale images, but small shifts occur from image to image. There are, however, also features in the images that become much less pronounced and change randomly. The movement of conductance maxima can be seen as diagonal patterns over the whole magnetic field range in some gate voltage regions. This wavelike pattern can be seen at the top of Figs. 6(c) and 6(d), whereas is not seen in Fig. 6(a). The geometric form of the dot alters when the gate voltage on one pair is changed. The form may be elliptic, with the size and eccentricity varying as a function of gate voltage. The form of the boundary changes, but not sufficiently to destroy the regularities of the conductance variations at zero magnetic field.

Alternative ways to test any correlation are to present the data in the form of power spectra or autocorrelation functions. We have analyzed fast-Fourier-transform (FET) power spectra of conductance variations as a function of magnetic field when the voltage on one gate pair is varied. High amplitudes of FFT's are observed for low-frequency variations of the magnetoconductance. The spectra, however, are difficult to interpret and analyze. A small variation in gate voltage changes the distribution of spectral peaks mainly in amplitude, but small shifts of positions are also observed. We have chosen not to average or smooth the spectra (narrow peaks may be insignificant when smoothed). Instead we transform a number of mag-

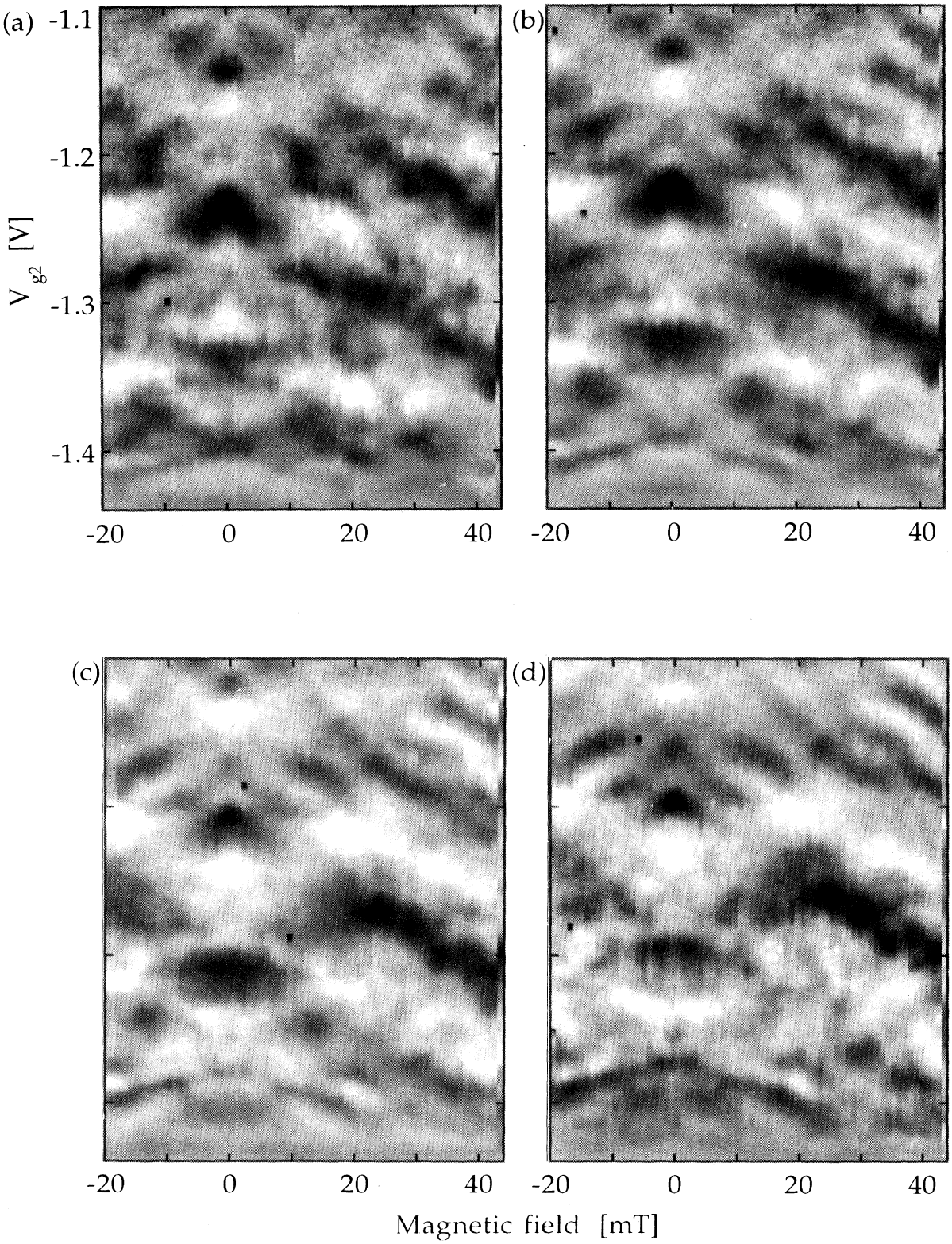

FIG. 6. Conductance variations as a function of V_{g2} and magnetic field, with higher conductance shown bright and lower conductance dark. From left: (a) $V_{g1}=-1.31$ V, (b) $V_{g1}=-1.32$ V, (c) $V_{g1}=-1.33$ V, and (d) $V_{g1}=-1.34$ V.

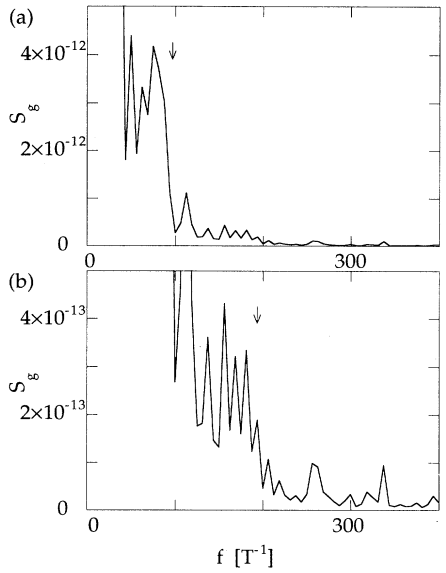

FIG. 7. The maximum amplitudes of 20 FFT power spectra of magnetoconductance traces plotted on a linear scale. Two steps, marked with arrows, can be seen, where the amplitude decreases approximately one order of magnitude. Only the y-axis scale has been changed between (a) and (b). V_{g2} is varied in a range from $V_{g2}=-1.410$ to -1.372 V, and $V_{g1}=-1.310$ V. The total change in radius is approximately 13 nm for this range.

netoconductance traces within a small range of the gate voltage and show the maximum values of these as a function of magnetic frequency, giving an envelope for the amplitudes.

The result is shown on a linear scale in Fig. 7 and on a logarithmic in Fig. 8. As shown in the latter, there is a general, roughly exponential, decay of the maximum amplitude with magnetic frequency. However, in our case the decrease is not featureless. The amplitude significantly decreases at $f=100$ T^{-1} (marked with an arrow in Fig. 7). This frequency corresponds to the Aharonov-Bohm frequency of a ring with radius $r=0.36$ μm.

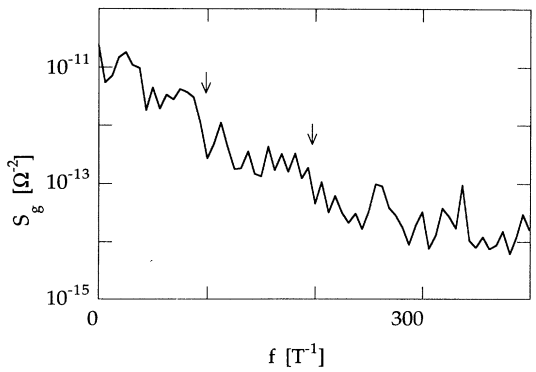

FIG. 8. Same data as in Fig. 7 but on a logarithmic scale, and with arrows at the same positions, indicating steps of approximately one order magnitude. The steps are naturally less pronounced on a logarithmic scale.

Another decrease is seen at twice that frequency in Fig. 7(b). These steps can be seen in the logarithmic plot of Fig. 8, but they are much less evident.

IV. ELECTRON TRANSPORT MODEL

We will now compare the experimental results with theoretical ones obtained with a simplified model, namely, that of a perfectly circular dot with no influence of contacts. The dominating characteristics of the experiments are a complex but regular variation of the conductance. Smaller effects arise from irregularities and cause random variations of the conductance. The observed small weak localization dip can be attributed to the irregularities of the boundary. The energy spectrum will first be calculated and we will find that the energy levels will tend to coincide at different energies, giving rise to peaks in the electron density of states. The eigenenergy levels are affected by an applied magnetic field. Knowing the electron density of states, the conductance of a dot connected weakly to two reservoirs can be calculated. The leads represent a perturbation of the individual electron states, but although the levels become Lorentzian broadened the level structure remains essentially intact when the leads are opened.

A. The energy spectrum

The energy levels of the dot are obtained by solving the Schrödinger equation $H\Psi(r,\theta)=E\Psi(r,\theta)$ in cylindrical coordinates, with a hard-wall confinement at $r=a$. The magnetic field is in the z direction and a symmetrical gauge $\mathbf{A}(r,\theta,z)=(0,rB/2,0)$ is chosen. The Hamiltonian can be written as

$$H=-\frac{\hbar^2}{2m^*}\left[\frac{1}{r}\frac{\partial}{\partial r}\left[r\frac{\partial}{\partial r}\right]+\frac{1}{r^2}\frac{\partial^2}{\partial\theta^2}+i\frac{eB}{\hbar}\frac{\partial}{\partial\theta}-\left[\frac{eBr}{2\hbar}\right]^2\right]. \quad (1)$$

This problem can be solved in weak magnetic fields by using perturbation theory.[26] This approximation is valid if the cyclotron radius $r_c=m^*v_F/eB$ is much smaller than the dot radius. v_F is the Fermi velocity and m^* is the effective mass of the electrons.

The perturbed eigenenergies are given by

$$E_{n,m}=E_0\left[\gamma_{n,m}^2+2n\alpha+\tfrac{1}{3}\alpha^2\left[1+\frac{2(n^2-1)}{\gamma_{n,m}^2}\right]\right], \quad (2)$$

$$E_0=\frac{\hbar^2}{2m^*a^2},$$

where the magnetic field dependence enters in $\alpha=\pi a^2Be/h$, the flux through the dot with radius a normalized to the magnetic flux quantum. They are related to the zeros of the Bessel functions $\gamma_{n,m}$, where the index m denotes the number of the root to the nth-order Bessel functions, $J_n(\gamma_{n,m})=0$, $n=0,\pm1,\pm2,\ldots$, and $m=1,2,\ldots$. E_0 corresponds to the average spacing between levels in the dot.

A few levels are plotted as a function of magnetic field in Fig. 9(a) in order to visualize the origin of regions with high density of states. Two levels $E_{n,m}$ of zeroth order; $(n,m)=(0,20)$ and (0,19), are drawn in Fig. 9. They have only a weak quadratic magnetic field dependence due to the cancellation of the second term in Eq. (2). There are several other levels that are close in energy to (0,19) and (0,20) around $B=0$. These are of even order in n, exemplified by $(\pm 2,19)$ and $(\pm 4,18)$ in the diagram. It is possible to draw a curve that touches all the curves of energy versus magnetic field tangentially. In analogy with optics, this curve is called a "caustic" and it passes a region of high density of electron states. Similarly, it is possible to draw a caustic to the (0,19) region. Between these two caustics are the levels $(-1,19)$ and (1,19) which also have a weak magnetic field dependence. Close in energy to these are other odd n states [exemplified by $(\pm 3,18)$ and (5,17) in Fig. 9]. The odd levels give rise to another caustic. Thus it is possible to map gently sloped, parabolic bands of high electron density of states in energy versus magnetic field diagrams. The magnetic field dependence is stronger for higher-order levels, giving a larger slope, as illustrated in the figure by a few lowest-order-in-m roots of high order in $n, n=51,52$.

The energy spectrum is affected by the dot size [see Eq. (2)]. The whole spectrum will change and regions of high density of states will pass through the Fermi energy when the radius is varied. Traces are drawn to describe the resonance conditions $E_{n,m}=E_F$, in Fig. 9(b), for the same levels as in Fig. 9(a). The lines give the variation in radius as a function of magnetic field, where the condition is valid. In an experiment, both area and depth of the potential well vary as a function of gate voltage. The small difference between Figs. 9(a) and 9(b) shows that calculating the conductance as a function of radius, or as a func-

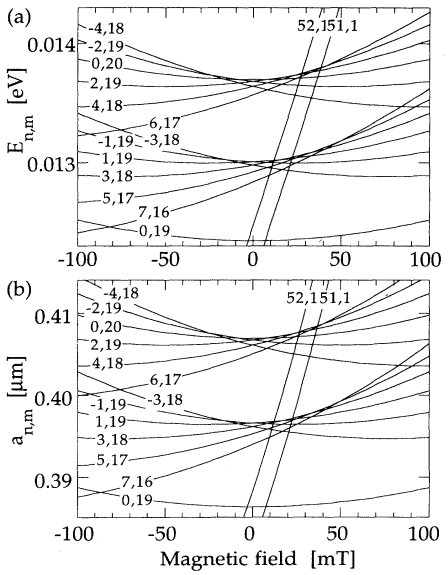

FIG. 9. (a) $E_{n,m}$ vs B. The levels are marked with quantum numbers: the order n and root m. $a=0.4$ μm. The levels (0,19) and (0,20) show the change of energy between different roots for zero-order levels. The levels (52,1) and (51,1) show the change between the first root of highest-order levels, both in energy and the periodicity in magnetic field. In (b), the dot radii $a_{n,m}$, which give a resonance condition $E_{n,m}=E_F=13.2$ meV, are plotted as a function of magnetic field.

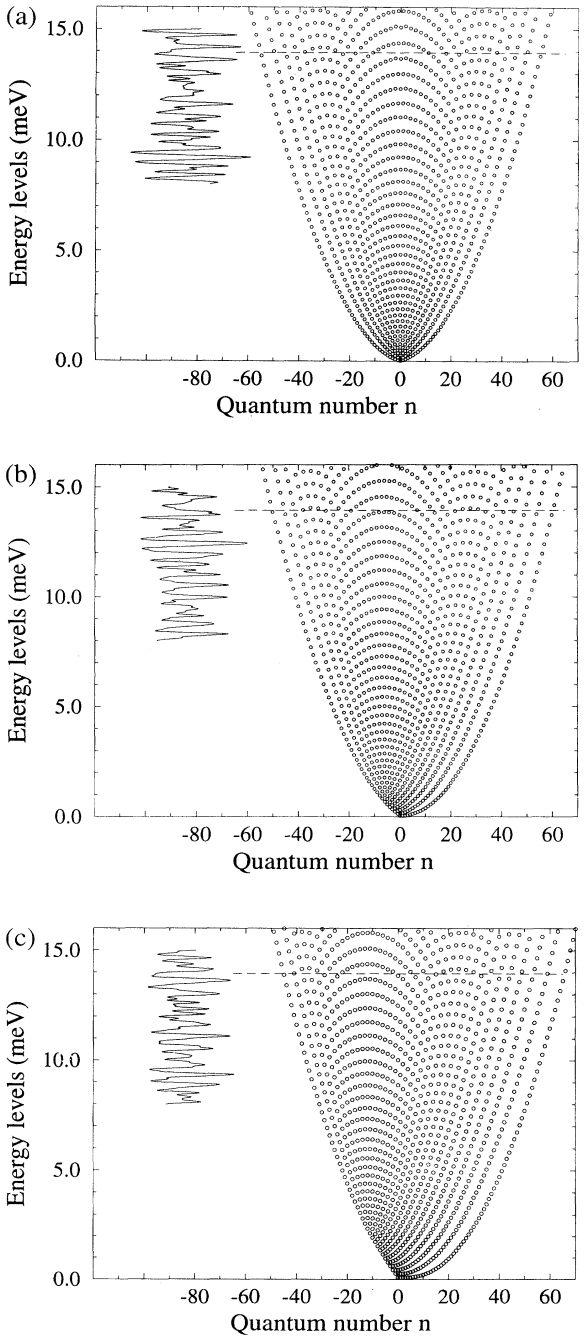

FIG. 10. (a)–(c) Energy diagrams at (a) $B=0$ T, (b) $B=-50$ mT, and (c) $B=-100$ mT. The energy of each state is plotted as a function of its quantum number n. The ordering of levels in inverted parabolas results in recurrently appearing maxima of the density of states and corresponding peaks of the conductance. The conductance traces shown to the left, with arbitrary unit, are calculated for $T=400$ mK.

tion of depth of the potential, gives the same spectral information. The complexity of the spectrum can be seen in Fig. 11, a calculation of conductance as a function of radius and magnetic field at low temperatures, where single level resonances [corresponding to $a_{n,m}(B)$ in Fig. 9(b)] are resolved and prominent parabolic caustics can be seen.

The energy levels are plotted versus the quantum number n, for magnetic fields $B=0$, -50, and -100 mT, in Figs. 10(a)–10(c). Energies where the density of states is high can easily be recognized in these diagrams, i.e., at the top of inverted parabolas. The states forming an inverted parabola around $n=0$, just below the line through $E=14$ meV, are those that contribute to the top caustic in Fig. 9. The tops of the parabolas shift to the left and to higher energies when the perturbing negative magnetic field is applied. The high-order levels also form parabolas, but they have a stronger linear magnetic field dependence and result in diagonal caustics (levels with positive n have positive slope).

B. Conductance calculation

The dot is connected to two reservoirs and the conductance can be calculated with a Landauer-type formula where we assume that the levels are Lorentzian broadened:

$$G=\frac{2e^2}{h}\int dE\left[-\frac{df}{dE}\right]T(E)$$
$$\propto\frac{e^2\Gamma}{\hbar k_B T}\sum_{n,m}\frac{\eta_{n,m}}{(1+\eta_{n,m})^2}\ , \tag{3}$$

where $\eta_{n,m}=\exp[(E_{n,m}-E_F)/k_BT]$ and $T(E)$ is the transmission probability for states at the energy E. We assume that the transmission probability is equal for all states and the thermal broadening k_BT is larger than the Lorentzian broadening Γ. (This is not the case for strong magnetic fields, where the transmission probability is higher through the outermost edge state.) Equation (3) relates the conductance to the density of states of the dot, with the thermal smearing determined by the derivative of the Fermi-Dirac function df/dE.

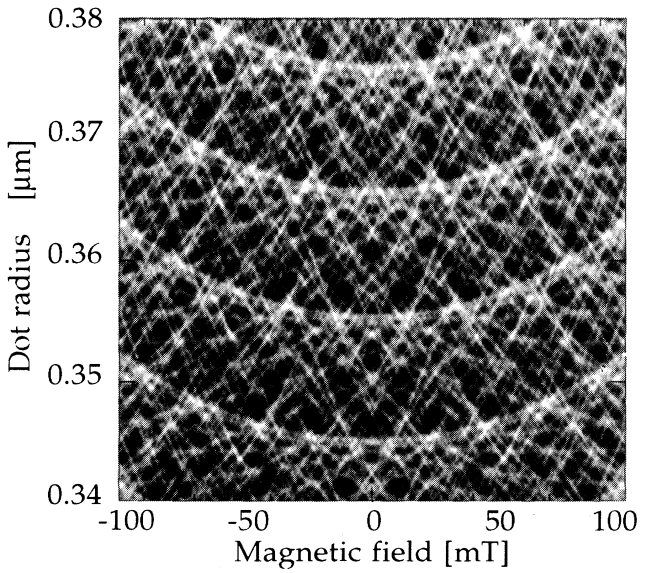

FIG. 11. Calculated conductance as a function of radius and magnetic field, at 100 mK. Compare with Fig. 7(b), where a few resonance lines $a_{n,m}(B)$ derived from the relation $E_{n,m}=E_F$ are plotted.

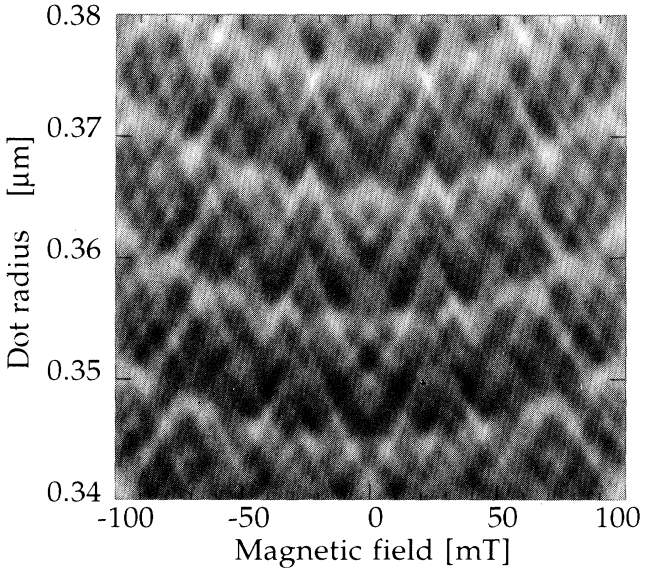

FIG. 12. Calculated conductance as a function of radius and magnetic field at $T=400$ mK. In this grey scale the resonant levels are smeared and overlap.

The regularity of conductance variations originates from recurrent crossings of coincident levels with the Fermi energy. The regularity is not clearly seen when the temperature is low, as every level causes a conductance peak of equal height. The individual levels are smeared at higher temperature and regions with high density of states become visible in the conductance. In Fig. 10, peaks in conductance occur at the same energy as where tops of inverted parabolas are located in the level dia-

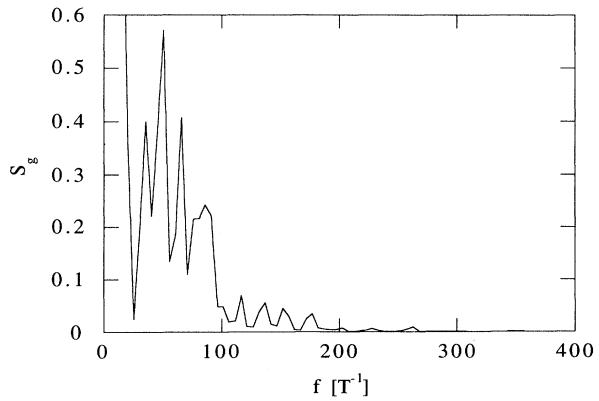

FIG. 13. Same spectra as in Fig. 14 but with logarithmic y axis. A generally exponential decay of amplitudes can be seen, but with a stepwise drop at $f=100$ T^{-1}.

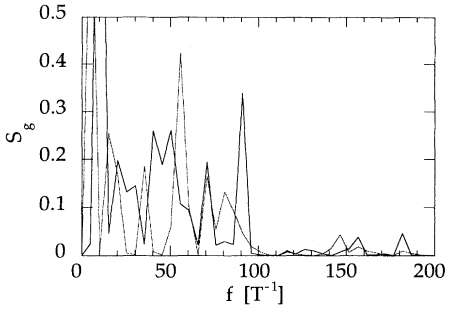

FIG. 14. Power spectra of calculated magnetoconductance. $a=0.3400$ μm and $a=0.3404$ μm. Even a small change of radius makes significant changes of the spectra: peaks shift and amplitudes change.

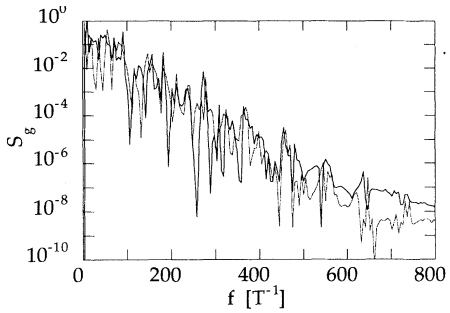

FIG. 16. Same as in Fig. 15 but on a logarithmic scale, and normalized to fit the experimental data of Fig. 8 (grey line). Drops in amplitudes at 100 and 200 T^{-1} are marked by arrows.

gram. The conductance as a function of both magnetic field and dot radius is shown as grey-scale images in Fig. 11 for $T=100$ mK and in Fig. 12 for $T=400$ mK. A bright image indicates high conductance. In Fig. 11, the thermal smearing is not pronounced and single level resonances can be distinguished, whereas in Fig. 12 only peaks in conductance due to coincident levels are seen. Caustics from low order n are seen as recurrently appearing inverted parabolas of high conductance. The diagonal pattern, with both positive or negative slopes, is due to coincidences of levels with larger positive or negative n values.

The theoretical magnetoconductance has, like the experimental, been analyzed with fast-Fourier-transform power spectra. The power spectrum has been predicted to decay exponentially at high magnetic frequencies for a chaotic quantum dot.[8] As shown in Fig. 13, we indeed find a generally exponential decay of amplitudes, but in addition there are frequencies where the amplitude decreases stepwise. The power spectra of single sweeps change when the radius is slightly varied (see Fig. 14). The amplitudes of some peaks increase, whereas other peaks get smaller. The variation of peak heights as a function of dot radius can be predicted with periodic orbit theory.[27]

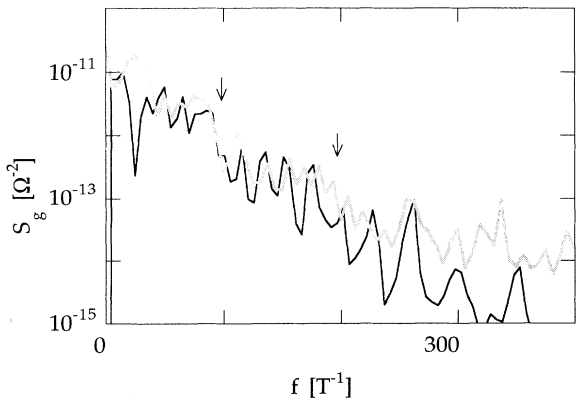

FIG. 15. The maximum amplitudes max[$Sg(f,a)$] of 25 power spectra of calculated magnetoconductance at $T=0.4$ K, where the radius a is varied from 0.36 to 0.37 μm.

To get a more clear picture, we calculate the power spectra for several theoretical magnetoconductance sweeps corresponding to small changes in the dot radius and plot an envelope representing the maximum values of the amplitude as a function of magnetic frequency. This is shown on a linear amplitude scale in Fig. 15 for 25 sweeps of magnetoconductance where the dot radius was changed from 0.36 to 0.37 μm. A rapid decrease of the envelope of the power spectra with magnetic frequency is noted. However, there is also a marked step in amplitude at $f\approx 100$ T^{-1}. This is of the same order as in experimental data, as shown on a logarithmic scale in Fig. 16.

The large amplitude of low-frequency components can be explained. The energy levels of the dot change and cross the Fermi, when the magnetic filed is varied. These consecutively lead to conductance peaks. The shortest magnetic field period is due to levels $E_{n,m}$ with the strongest magnetic field dependence, namely, those with $m=1$ and high quantum number n (see Fig. 9). The period corresponds approximately to the addition of a magnetic flux quantum to the dot. Other levels with lower n have a weaker magnetic field dependence and cause conductance peaks with larger separations in field. The power spectra will therefore have high amplitudes for frequencies below the Aharonov-Bohm frequency $f=\pi a^2 e/h$, which, for a dot radius $a=0.36$ to 0.37 μm is $f\approx 100$ T^{-1}. This drop is seen in the power spectra (Figs. 15 and 16), where the maximum amplitude drop by one order of magnitude at $f=100$ T^{-1} and a second drop is seen at twice that frequency.

V. DISCUSSION

We have found that the energy levels of a perfectly circular disk can be used to model the conductance variation of a quantum dot in a two-dimensional electron gas. There is qualitative agreement between experimental and numerical conductance traces. The conductance variations, as a function of size and magnetic field, are characterized by coincidence of energy levels into "caustics." When the magnetic field is varied, these caustics cause low-frequency variations of the conductance. The most pronounced regularity is large conductance variations when the gate voltage is varied, which is due to energy levels with low quantum number n that coincide in a kind

of shell structure.[28] In relation to the semiclassical "billiard ball" model, these low n states correspond to an electron bouncing back and forth in the dot. As the trajectories do not enclose any flux, these levels have only a weak magnetic field dependence due to bending of the electron trajectories by the Lorentz force. The highest n level can be seen as a trajectory of an electron that bounces very close to the boundary. It encloses almost the entire area of the dot and has therefore a stronger magnetic field dependence.

A large dot with many electrons contains many possible trajectories. The most prominent trajectory is the pendulum motion, the next is triangular, then square, etc., all enclosing different areas. Each of these levels will have a periodicity in magnetic field due to the Aharonov-Bohm effect. Our model gives a similar result of recurrently appearing states giving resonant conditions, with the strongest field dependence of the highest-order levels. The large changes of magnetoconductance between traces with modest variations of the radius may be mistaken for being uncorrelated due to the complexity and difference in magnetic field dependencies of the states.

The shell structure with recurrently appearing energies with a high density of states results in conductance variations that are seen at temperatures up to several Kelvin even though the average separation between levels is smaller than thermal fluctuations The energy separation between the shells with coincident levels is, as seen in Fig. 10, slightly smaller than 1 meV, which corresponds to thermal fluctuations at 10 K.

The analyses of magnetoconductance power spectra generally give an exponential decay of amplitudes for high frequencies. The exponential decay is very similar to the semiclassical prediction for a chaotic system.[8] It should be noted though that it agrees even with our calculations, which are nonchaotic. We can, however, also see stepwise decreasing amplitudes for low frequencies. Steps are not necessarily seen in the power spectrum of an individual experimental or theoretical magnetoconductance trace; but looking at maximal peak heights of power spectra, steps occur at frequencies corresponding to adding integral fractions of flux quanta through the area of the dot. If we consider either classical trajectories or Bessel function orbits, each state will enclose different effective areas. The largest enclosed area for a single orbit is the dot area πa^2, for an orbit twice around the dot it is $2\pi a^2$, and so forth. The contribution to the conductance from a single loop trajectory is higher than from a multiturn loop. Therefore, we see a higher amplitude of components with frequencies lower than $f=\pi a^2 e/h$, corresponding to additions of single flux quanta to the dot. We can only see two steps in the experimental power spectra. This may be due to elastic and inelastic scattering events changing the trajectory. The second step corresponds to electron with trajectories going twice around the perimeter (enclosing twice the dot area). This is comparable to the mean free path of our dot. We cannot assume regularities of conductance oscillations of higher frequencies, where the electron path must be longer than the mean free path.

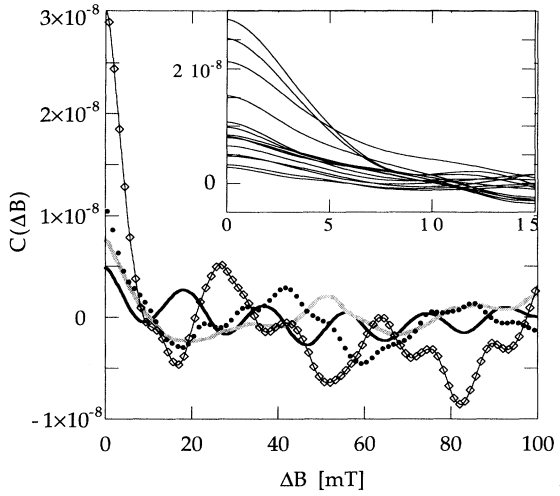

FIG. 17. The autocorrelation of experimental magnetoconductance sweeps. Four curves are shown for the same data as used for the experimental power spectra in Figs. 7 and 8. The inset shows autocorrelation for 15 traces in the same range. There is no universal form of autocorrelation of experimental data.

Autocorrelation functions have been used to analyze the energy spectrum of chaotic systems, and a universal form has recently been predicted.[11,29,30] We calculated autocorrelation of magnetoconductance sweeps for both experimental and calculated data. The form of the correlation function changes drastically between different sweeps for which the gate voltage (dot size) has been changed slightly; see Figs. 17 and 18. The form is not universal, and in some cases there is a clearly periodic correlation. We can therefore conclude that for the inte-

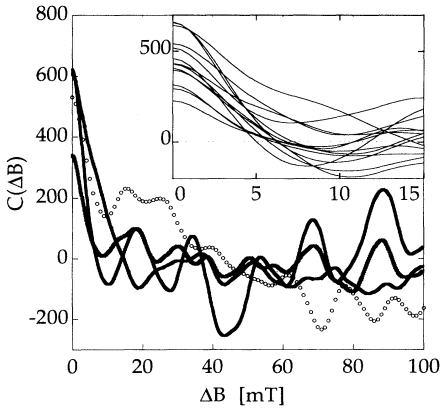

FIG. 18. Autocorrelation of numerical magnetoconductance sweeps, for different radius ($a=0.3452$, 0.3462, 0.3482, 0.3492 μm) at 0.4 K (arbitrary y scale). The form of the correlation function changes and the width of the zero peak varies when the radius changes even a small amount. There is no universal form of the numerical autocorrelation functions. The inset shows a number of autocorrelation traces, where the radius is changed within the interval 0.34–0.35 μm.

grable system we do not find a universal form of the autocorrelation.

A signature of chaos can, in our opinion, be observed most directly in our grey-scale images of the measurements. Chaos will break the coincidence of energy levels from caustics and spread them more evenly, diminishing the regular variations of the density of states. In Fig. 6, the first image ($V_{g1}=-1.31$ V) represents a more chaotic system than, for example, the third ($V_{g1}=-1.33$ V), since the short-period diagonal patterns that correspond to trajectories along the perimeter (or levels with high quantum number n) are almost completely washed out. The longer period structure of dark and white spots, which correspond to orbits with fewer bounces (low n), is not as sensitive to the shape of the dot.

VI. CONCLUSION

Our study shows that the experimental magnetoconductance of a quantum dot can be modeled by a simplified model, in which the energy eigenvalues of a circular dot are calculated as functions of magnetic field and dot size. We have not taken into account the influence of contacts that are difficult to model in a magnetic field. Qualitatively, there exists a strong resemblance between the general behavior of the experimental and simulated conductance as functions of magnetic field and dot size. Individual magnetoconductance curves vary drastically as the gate voltages, the size, or form of the dot are changed slightly. Seemingly, there is no correlation. However, a grey-scale image of the conductance as a function of both field and size shows regions of characteristic, nonchaotic behavior. These conductance variations can be traced to coincident levels in the energy diagram of the dot. With this simple model it is possible to extend the comparisons between experimental and calculated data to more complex geometries than a circular one.

Individual power spectra of the magnetoconductance also vary from trace to trace depending upon small changes in the confinement. There is a general, exponential decay of the average amplitude with magnetic frequency. However, we have discovered that it is possible to distinguish steps in the power spectra at characteristic frequencies, corresponding to integral fractions of flux quanta through the dot, if many spectra are superimposed and one considers the envelope of the maxima of the power spectra amplitudes. This was the case for both the experimental and the calculated curves but only two steps could be traced in the experimental situation. This is probably due to the limitation set by a finite mean free path of the electrons in the dot.

ACKNOWLEDGMENTS

We have benefited from discussions with M. Jonson and P. Delsing and the technical assistance from M. Bøgelund and C. Sørensen. We utilized the Swedish Nanometer Laboratory for electron beam lithography. The work was supported by the Swedish Board of Technical and Industrial Development, the Swedish Research Council for Engineering Sciences, and the Swedish and the Danish Natural Science Research Councils.

[1]M. A. Kastner, Phys. Today **46** (1), 24 (1993).
[2]R. C. Ashoori, H. L. Stormer, J. S. Weiner, L. N. Pfeiffer, K. W. Baldwin, and K. W. West, Surf. Sci. **305**, 558 (1994).
[3]P. L. McEuen, E. B. Foxman, U. Meirav, M. A. Kastner, Y. Meir, N. S. Wingreen, and S. J. Wind, Phys. Rev. Lett. **66**, 1926 (1991).
[4]U. Meirav, P. L. McEuen, M. A. Kastner, E. B. Foxman, A. Kumar, and S. J. Wind, Z. Phys. B **85**, 357 (1991).
[5]P. L. McEuen, E. B. Foxman, J. Kinaret, U. Meirav, M. A. Kastner, N. S. Wingreen, and S. J. Wind, Phys. Rev. B **45**, 11 419 (1992).
[6]R. C. Ashoori, H. L. Stormer, J. S. Weiner, L. N. Pfeiffer, K. W. Baldwin, and K. W. West, Phys. Rev. Lett. **71**, 613 (1993).
[7]M. Robnik, J. Phys. A **17**, 1049 (1984); M. V. Berry and M. Robnik, *ibid.* **19**, 649 (1986).
[8]R A. Jalabert, H. U. Baranger, and D. Stone, Phys. Rev. Lett. **65**, 2442 (1990).
[9]R. A. Jalabert, D. A. Stone, and Y. Alhassid, Phys. Rev. Lett. **68**, 3468 (1992).
[10]A. D. Stone and H. Bruus, Physica B **189**, 43 (1993).
[11]A. D. Stone and H. Bruus, Surf. Sci. **305**, 490 (1994).
[12]C. M. Marcus, A. J. Rimberg, R. W. Westervelt, P. F. Hopkins, and A. C. Gossard, Phys. Rev. Lett. **69**, 506 (1992).
[13]C. M. Marcus, R. M. Westerwelt, P. F. Hopkins, and A. C. Gossard, Phys. Rev. B **48**, 2460 (1993).
[14]M. W. Keller, O. Millo, A. Mittal, D. E. Prober, and R. N. Sacks, Surf. Sci. **305**, 501 (1994).
[15]M. J. Berry, J. A. Katine, C. M. Marcus, R. W. Westervelt, and A. C. Gossard, Surf. Sci. **305**, 495 (1994).
[16]C. M. Marcus, R. M. Westervelt, P. F. Hopkins, and A. C. Gossard, Surf. Sci. **305**, 480 (1994).
[17]A. A. M. Staring, B. W. Alphenaar, H. van Houten, L. W. Molenkamp, O. A. J. Buyk, M. A. A. Mabesoone, and C. T. Foxon, Phys. Rev. B **49**, 12 869 (1992).
[18]C. W. J. Beenakker and H. van Houten, in *Solid State Physics,* edited by H. Ehrenreich and D. Turnbull (Academic, San Diego, 1991).
[19]L. Glazman and M. Jonson, Phys. Rev. B **41**, 10 686 (1990).
[20]Y. Aharonov and D. Bohm, Phys. Rev. **115**, 485 (1959).
[21]P. A. Lee and A. D. Stone, Phys. Rev. Lett. **55**, 1622 (1985).
[22]See Z. Phys. B **85** (3) (1991), special issue on single charge tunneling.
[23]H. van Houten, C. W. J. Beenakker, and A. A. M. Staring, in *Single Charge Tunneling,* Vol. 294 of NATO Advanced Study Institute, Series B: Physics, edited by H. Grabert and M. H. Devoret (Plenum, New York, 1992).
[24]B. J. van Wees, L. P. Kouwenhoven, C. J. P. M. Harmans, J. G. Williamson, C. E. Timmering, M. E. I. Broekaart, C. T. Foxon, and J. J. Harris, Phys. Rev. Lett. **62**, 2523 (1989); L. Kouwenhoven *et al.*, Surf. Sci. **229**, 290 (1990).
[25]M. Persson, Ph.D. thesis, Chalmers University of Technology, 1994, p. 95.

[26]R. B. Dingle, Proc. R. Soc. London Ser. A **212**, 47 (1952).
[27]S. M. Reimann (private communication).
[28]P. E. Lindelof, A. Kristensen, and M. Persson, *Coulomb and Interference Effects Small Electronic Structure* (Editions Frontières, Gif sur Yvette, 1994).
[29]B. D. Simons and B. L. Altshuler, Phys. Rev. Lett. **70**, 4063 (1993).
[30]A. Szafer and B. L. Altshuler, Phys. Rev. Lett. **70**, 587 (1993).

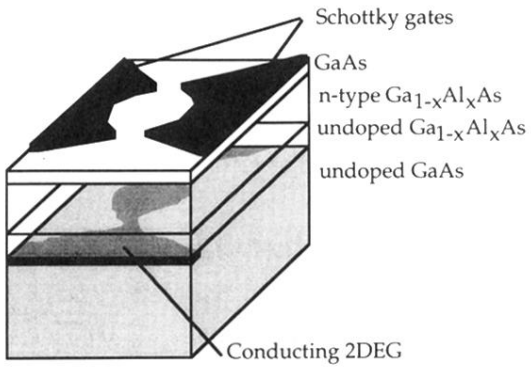

FIG. 1. Schematic layer configuration of the heterostructure. A high mobility 2DEG forms in the undoped GaAs at the interface to the $Ga_xAl_{1-x}As$ layer. The 2DEG is separated from the randomly distributed donors in the $Ga_xAl_{1-x}As$ by an undoped spacer layer. A negative voltage V_g on the gates depletes the 2DEG beneath the gates.

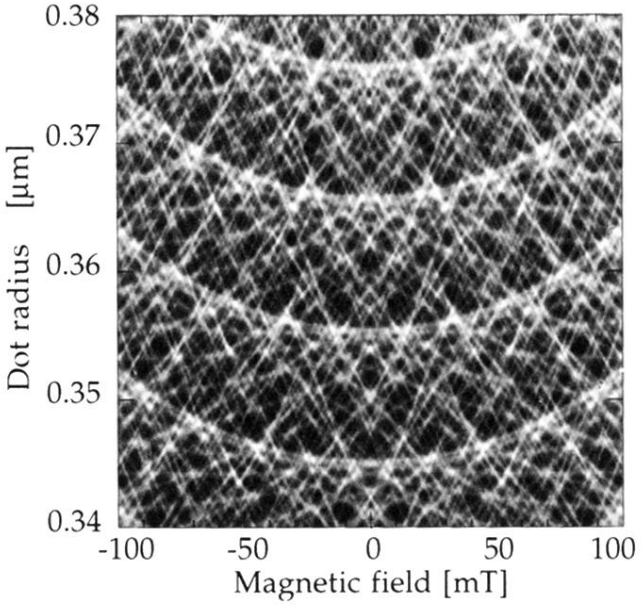

FIG. 11. Calculated conductance as a function of radius and magnetic field, at 100 mK. Compare with Fig. 7(b), where a few resonance lines $a_{n,m}(B)$ derived from the relation $E_{n,m}=E_F$ are plotted.

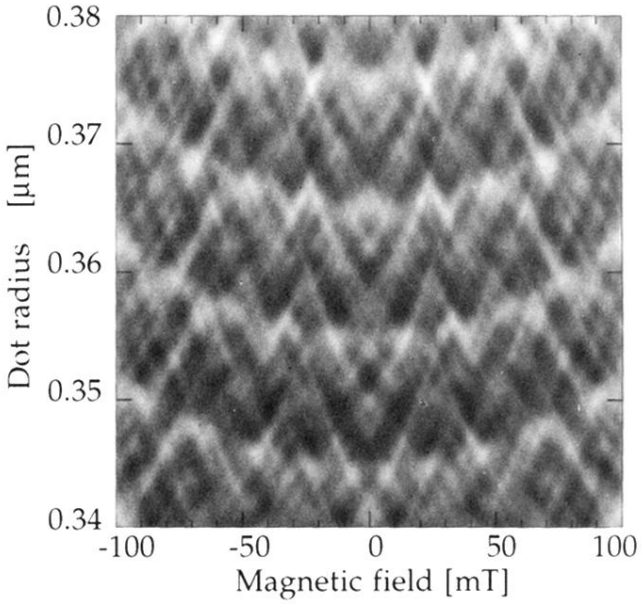

FIG. 12. Calculated conductance as a function of radius and magnetic field at $T=400$ mK. In this grey scale the resonant levels are smeared and overlap.

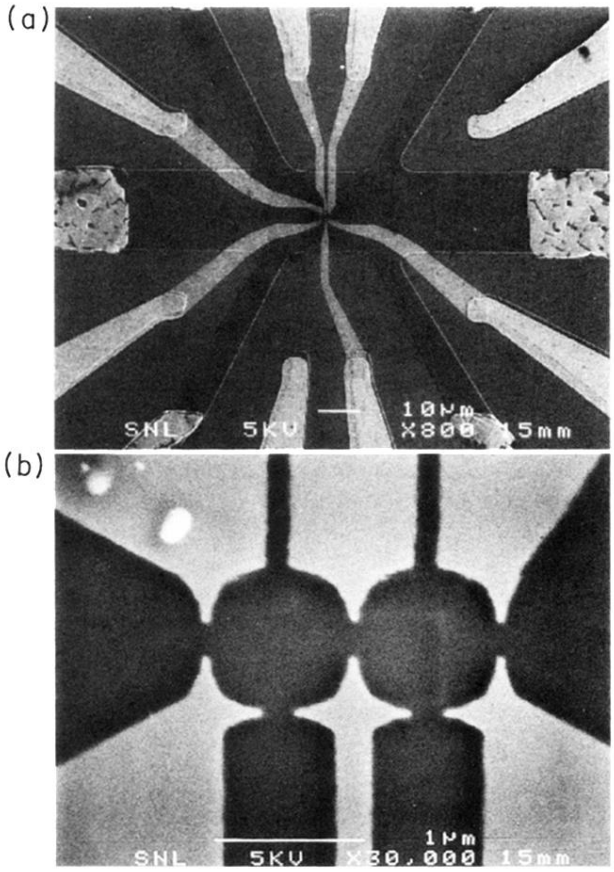

FIG. 2. (a) Scanning electron microscope (SEM) image of the device with gates and Ohmic contacts shown. (b) SEM image of the gate structure. Two gate pairs were used during the measurements, the third was grounded or disconnected. The gate voltages V_{g1}, V_{g2}, and V_{g3} referred to in the text are the voltages applied to the two right gates, to the middle gates, and to the left gates, respectively. The gates can form three individually adjustable quantum point contacts and two circularly shaped quantum dots.

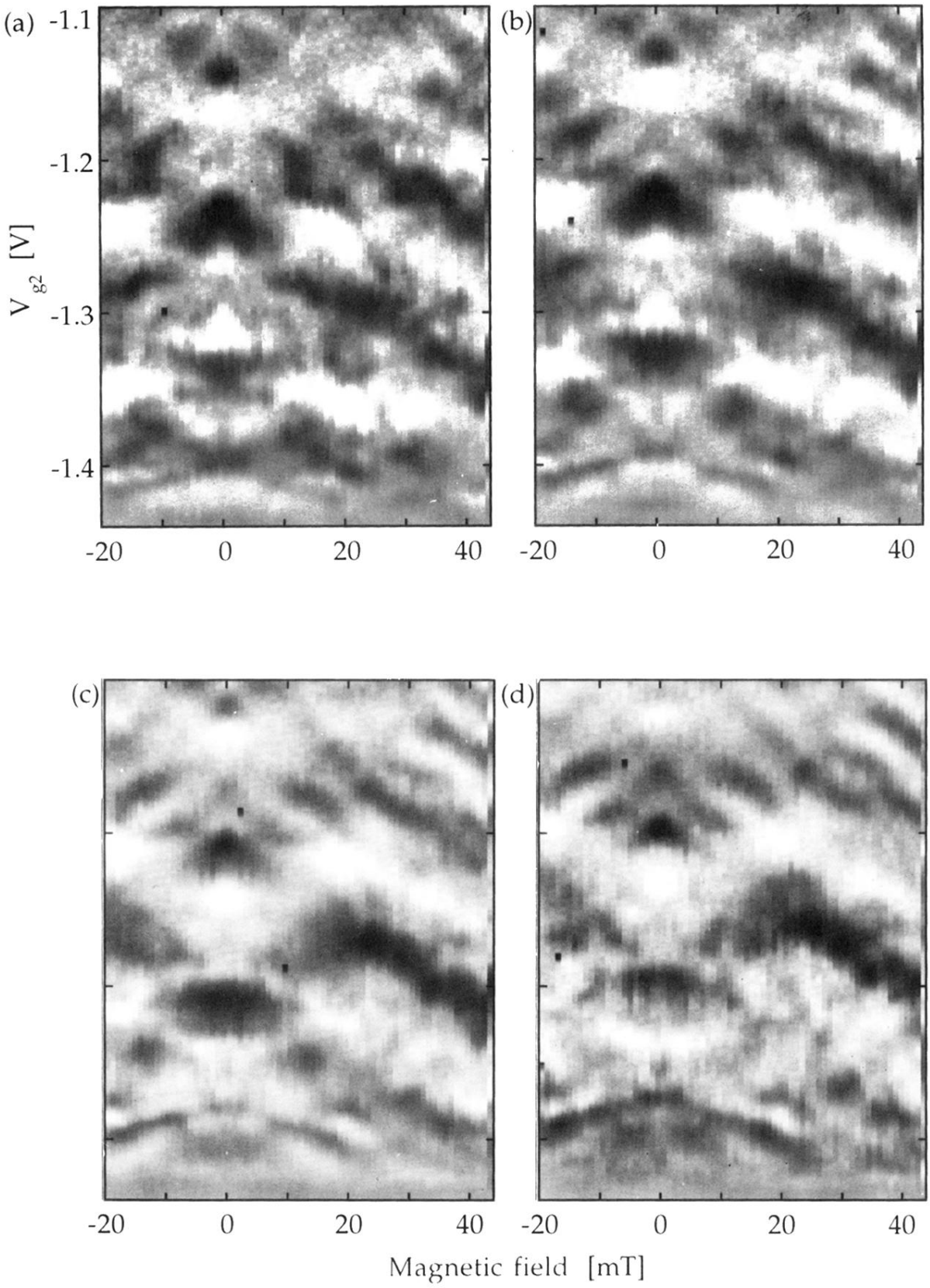

FIG. 6. Conductance variations as a function of V_{g2} and magnetic field, with higher conductance shown bright and lower conductance dark. From left: (a) $V_{g1} = -1.31$ V, (b) $V_{g1} = -1.32$ V, (c) $V_{g1} = -1.33$ V, and (d) $V_{g1} = -1.34$ V.